


## Research Article

## A Comprehensive Study on the Effect of Wire EDM Current Intensity on the Tribological Behavior and Energy Efficiency in Aluminum Machining: A Novel Approach Toward Sustainable Manufacturing

Ramezan Ali Mahdaveinejad<sup>1\*</sup>, Sayyed Mohammadreza Sedehi<sup>1</sup> , Seyyed Nabi Al-din Sharifi<sup>2</sup> and Amirmohammad Dastmard<sup>3</sup>

<sup>1</sup> School of Mechanical Engineering, College of Engineering, University of Tehran, Tehran, Iran

<sup>2</sup> Faculty of Engineering, Najafabad Branch, Islamic Azad University, Najafabad, Iran

<sup>3</sup> Department of Engineering, Islamic Azad University, Mashhad, Iran

## ARTICLE INFO

*Article history:*

Received: 22 July 2025

Reviewed: 25 August 2025

Revised: 9 September 2025

Accepted: 28 September 2025

*Keywords:*

Wire EDM

Aluminum

Tribological behavior

Energy

Current intensity

*Please cite this article as:*

Mahdaveinejad, R. A., Sedehi, S. M., Sharifi, S. N. A. & Dastmard, A. (2025). A Comprehensive study on the effect of wire EDM current intensity on the tribological behavior and energy efficiency in aluminum machining: A novel approach toward sustainable manufacturing. *Iranian Journal of Materials Forming*, 12(4), 66-80.

<https://doi.org/10.22099/IJMF.2025.53767.1339>

## ABSTRACT

This study investigates the influence of discharge current variations in the wire electrical discharge machining (WEDM) process on the surface properties and tribological behavior of aluminum components. Five aluminum samples were machined at current levels ranging from 1 to 5 amperes, and their surface roughness, microhardness, wear resistance, and corrosion rate were evaluated. Additionally, the energy consumption per unit volume of material removed was calculated. The results showed that as the current increased from 1 to 5 A, surface roughness initially rose from 1.8  $\mu\text{m}$  for the reference sample to a maximum of 3.5  $\mu\text{m}$ , then decreased to 2.5  $\mu\text{m}$  at the highest current. Surface microhardness increased from 49.8 HV in the reference sample to a maximum of 57 HV. Wear and corrosion rates, key indicators of surface performance, were 9.2 mg and 0.008 mm/year under optimal conditions, compared to 18.4 mg and 0.001 mm/year in the reference sample. Furthermore, specific energy consumption initially decreased but then increased at higher currents due to unstable sparks and re-melting effects. These findings provide valuable insights for optimizing electrical parameters in WEDM parameters to improve the performance and sustainability of machined aluminum components.

© Shiraz University, Shiraz, Iran, 2025

### 1. Introduction

Aluminum, as one of the most widely used non-ferrous

metals in modern industry, plays a fundamental role across diverse sectors, including automotive [1],

\* Corresponding author

E-mail address: [mahdavin@ut.ac.ir](mailto:mahdavin@ut.ac.ir) (R. A. Mahdaveinejad)

<https://doi.org/10.22099/IJMF.2025.53767.1339>

aerospace [2], defense [3], electronics [4], and packaging [5]. Due to its low density, high strength-to-weight ratio, excellent corrosion resistance, superior thermal and electrical conductivity, and high recyclability, aluminum has consistently attracted the attention of researchers and engineers [6–8]. In recent decades, the growing demand for lightweight yet durable components have significantly increased the importance of precision manufacturing and machining of aluminum alloys [9–12]. Among the advanced manufacturing techniques, wire electrical discharge machining (WEDM) has emerged as a highly effective method for the precise cutting and shaping of aluminum components [13, 14]. This non-conventional process employs controlled electrical discharges between a moving wire electrode and the workpiece, enabling the fabrication of complex geometries with high dimensional accuracy and surface integrity. Key advantages of WEDM include its ability to cut intricate shapes without mechanical forces, thus preventing deformation and residual stresses, as well as its capability to machine hard and brittle conductive materials [15, 16]. In industrial applications, WEDM-manufactured aluminum components are found in aerospace parts [17], precision hydraulic control system components [18], and customized heat sink plates in electronic devices [19]. Among the critical WEDM process parameters, discharge current directly influences not only the material removal rate and production speed but also the energy consumption and final surface quality of the machined part [20]. As current increases, discharge energy intensifies, altering both the removal rate and the morphology of surface micro-craters [21]. These changes, in turn, have two major implications. First, they increase energy consumption, raising concerns about production costs and environmental sustainability; second, they modify surface characteristics, significantly affecting tribological performance, including wear resistance, friction behavior, and long-term durability [22]. Therefore, identifying the optimal current range that balances production speed, surface quality, energy efficiency, and environmental impact remains a key research priority. In recent years, environmental considerations and energy

consumption have become integral to evaluating manufacturing technologies [23, 24]. The growing demand for sustainable production and a reduced carbon footprint highlights the need for in-depth analysis of machining parameters in relation to energy efficiency. In WEDM, particularly at high current levels, the increase in electrical energy consumption can not only lead to economic drawbacks but also generate excessive heat, over-evaporation of the dielectric fluid, and ultimately the release of harmful byproducts into the environment. Thus, comprehensive understanding of the process from both energy and ecological sustainability perspectives is of strategic importance. On the other hand, the surface quality and tribological properties of WEDM-machined aluminum are critical in determining durability and functionality in industrial applications [25]. Parameters such as surface roughness, surface layer hardness, micro-cracks, and re-solidified inclusions greatly influence frictional behavior and wear resistance [26–28]. These features are especially crucial for moving parts or components subjected to cyclic loading. Consequently, proper selection of WEDM parameters particularly current intensity plays a vital role in improving component lifespan and process sustainability. In this context, Kiyak [29] investigated the influence of pulse-on time, pulse-off time, wire feed rate, and workpiece thickness on surface roughness, hardness, and material removal rate. The findings revealed that carbon content on machined surfaces varied with processing parameters and that carbon enrichment was closely related to microhardness, emphasizing the need for parameter optimization based on target surface properties. Similarly, Reddy et al. [30] conducted experiments aimed at minimizing energy consumption and surface defects during WEDM of Al–Si metal matrix composites by optimizing slot width, material removal rate, and surface quality. Their analysis identified current as the dominant parameter affecting process performance. The novelty of the present study lies in its integrated multidimensional approach, in which the influence of electrical current variation (1 - 5 A) on machining rate, energy consumption, environmental impact, and surface and tribological

properties of aluminum components is simultaneously evaluated. This research aims to elucidate the interrelations among technical performance, energy efficiency, and surface integrity, thereby advancing sustainable and precision machining practices.

## 2. Materials and Methods

In this study, commercially pure aluminum with 99.5% purity and an average grain size of 45  $\mu\text{m}$  was used as the base material. The precise chemical composition of this alloy is presented in Table 1. As shown, the content of alloying elements is very limited, allowing a clearer investigation of the effects of the wire electrical discharge machining (WEDM) process on surface phases and mechanical properties. The samples were prepared in cubic form with dimensions of  $10 \times 10 \times 10$  mm, as shown in Fig. 1. To examine the effect of discharge current, the WEDM process was applied separately to five samples at current levels of 1, 2, 3, 4, and 5 A, while the unmachined specimen served as the control sample. The WEDM process parameters used in this study are listed in Table 2. All machining operations were carried out using a Charmilles wire cut 6030si machine equipped with a 0.25 mm diameter brass wire. To minimize the influence of external variables, parameters such as voltage, pulse duration, wire feed rate, and dielectric type were kept constant for all tests, and only the discharge current was varied as the independent variable. After machining, the samples underwent laboratory testing to evaluate their surface, structural, and mechanical properties.

To identify and compare phase changes caused by wire EDM at different current intensities, X-ray diffraction (XRD) analysis was performed on all samples, including the control (S-0) and the machined specimens (S-1 to S-5). The tests were conducted using an Explorer model X-ray diffractometer (GNR, Italy) operating at 40 kV, and 30 mA with Cu K $\alpha$  radiation ( $\lambda = 1.5406$  Å). The diffraction angle range was  $2\theta = 20^\circ$  to  $80^\circ$ , with a scan rate of  $2^\circ$  per minute and a step size of  $0.02^\circ$ . For data analysis, the main peaks from each sample were extracted and compared with reference data (PDF) from the ICDD database. For detailed analysis,

the main peak region ( $44.74^\circ$ ) was magnified to investigate subtle variations in peak intensity and width, enabling quantitative and qualitative assessment of the influence of current intensity in the WEDM process on the crystalline structure and surface phase composition. Surface roughness measurements were conducted according to ISO 25178-2:2012 [31] using an optical profilometer (WYKO NT9100). The measurements uncertainty is provided in Table 3. The uniformity of surface roughness ( $R_a$ ) across five areas along the thickness direction was selected as an indicator of surface quality consistency. A surface roughness ( $R_a$ ) contour map for the measured areas along the thickness direction is shown in Fig. 2. The uniformity of surface roughness was calculated using Eq. (1):

$$Sa = \frac{\text{Max}(Ra_1 - Ra_5) - \text{Min}(Ra_1 - Ra_5)}{\text{Ava.}(Ra_1 - Ra_5)} \quad (1)$$

**Table 1.** Specifications of the aluminum used

| Material                           | (%)  |
|------------------------------------|------|
| Al                                 | 99.5 |
| Si                                 | 0.25 |
| Fe                                 | 0.20 |
| Cu                                 | 0.05 |
| Mn                                 | 0.05 |
| V                                  | 0.05 |
| Other                              | 0.03 |
| Density ( $\text{g}/\text{cm}^3$ ) | 2.7  |

**Table 2.** Sample identification

| Sample        | Current intensity (A) |
|---------------|-----------------------|
| S-0 (Pure Al) | -                     |
| S-1           | 1                     |
| S-2           | 2                     |
| S-3           | 3                     |
| S-4           | 4                     |
| S-5           | 5                     |

The surface microhardness was measured using the Vickers method with an INNOVATEST NEXUS 8000XL hardness tester, applying a 9.807 N (equivalent to 1 kgf) load with a diamond pyramid indenter and a 15 s dwell time, following ASTM E92 (2020) standard [32]. To evaluate wear resistance, dry-pin-on-disk wear tests were conducted in a specialized laboratory according to ASTM G99 standard at room temperature, under a load of 5 N, for 3600 s, and at a rotational of 60 rpm, using a

steel pin as the counter-body [33]. Wear rate was determined by measuring the weight loss of each sample after a sliding distance of 280 m. Additionally, corrosion behavior was assessed through electrochemical tests, including open circuit potential (OCP) and Tafel polarization measurements, performed in a 3.5% NaCl solution according to ASTM G01.05 standard [34]. All tests were repeated three times for each sample to ensure repeatability, and average values were reported. To observe the microstructural changes after each stage of the experiments, the samples, cut perpendicular to the pressing direction, were examined using an inverted metallographic microscope (Meiji, Japan). To preserve actual surface morphology and avoid eliminating the effects of tool interaction and thermal influences generated during machining, no conventional polishing process was carried out. The samples were cleaned and then etched with a solution consisting of H<sub>2</sub>O (0.88), HF (0.02), and HNO<sub>3</sub> (0.1) in normalized volume percent, which enabled clear observation of the surface features without altering the original characteristics produced by machining.

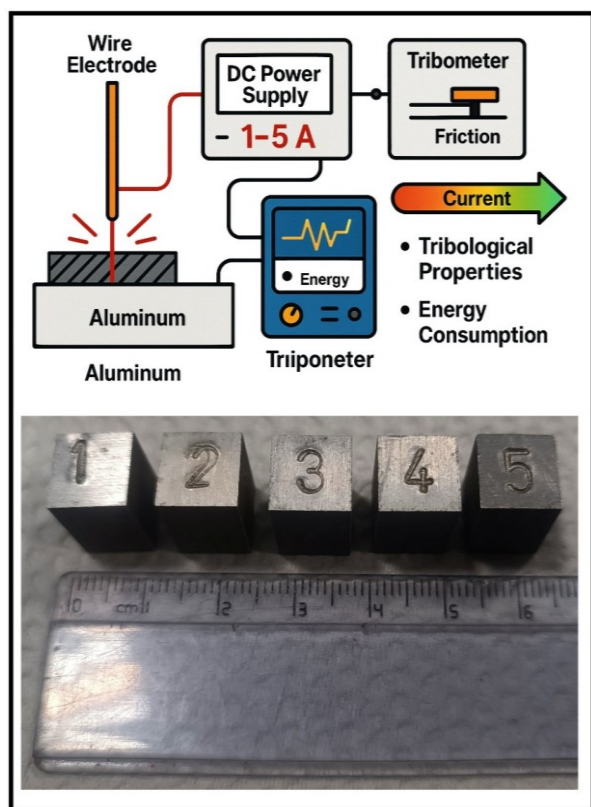


Fig. 1. Schematic of the WEDM process.

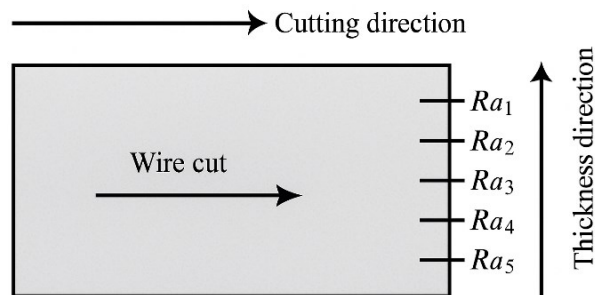


Fig. 2. Measured surface roughness (Ra) mapping of five regions.

Table 3. Uncertainty analysis of roughness test

| No. | Parameters                 | Value                |
|-----|----------------------------|----------------------|
| 1   | Vertical measurement range | 0.1 nm to 10 mm std. |
| 2   | Vertical resolution        | <0.1 nm              |
| 3   | RMS repeatability          | 0.05 nm              |
| 4   | Optical resolution         | 0.49 mm min          |
| 5   | Reflectivity               | <1e100%              |
| 6   | Step height                | 0.8% accuracy        |

### 3. Results and Discussion

#### 3.1. XRD analysis

The wire electrical discharge machining (WEDM) process, a precise non-contact technique for machining hard or thermally sensitive materials, significantly influences the microstructural and phase composition of aluminum surfaces. In this study, electrical current intensity (1–5 A) was examined as the primary variable to evaluate its influence on crystallographic changes and surface phase formation, as shown in Fig. 3. The reference sample (S-0), representing pure aluminum, exhibited the characteristic diffraction peaks of the face-centered cubic (FCC) Al phase at 38.47°, 44.74°, 65.13°, and 78.22° [33]. At elevated discharge currents, additional peaks corresponding to secondary phases were detected. The emergence of Al<sub>2</sub>O<sub>3</sub> peaks at 25.6° and 35.1° in samples S-1 and S-2 can be attributed to surface oxidation caused by localized high temperatures and exposure to oxygen during processing [35]. At 3 A, AlN peaks were observed at 36° and 33.1°, which are most likely formed due to nitrogen incorporation from the surrounding dielectric fluid and ambient atmosphere under plasma-assisted thermal activation [36]. For

samples machined at higher currents (S-4 and S-5), intermetallic phases such as AlCu and Al<sub>3</sub>Ni were identified. These compounds are plausibly derived from the diffusion of alloying elements originating from the brass wire electrode (Cu and Zn) and surface contamination from electrode impurities and dielectric breakdown products. The presence of Ni is likely associated with trace contamination from either the electrode composition or machine components in direct contact with the machining zone, which under repeated discharges can promote diffusion into the molten surface layer.

Overall, the formation of such phases strongly depends on the interaction between the molten aluminum surface, electrode material, and dielectric environment. While hard phases like Al<sub>2</sub>O<sub>3</sub> and AlN

enhance hardness and wear resistance, the presence of brittle intermetallic (e.g., AlCu) may reduce toughness and increase susceptibility to cracking. Therefore, careful adjustment of WEDM current is essential not only to ensure dimensional accuracy but also to manage surface phase evolution, enabling the tailoring of material properties for advanced engineering applications.

### 3.2. Surface roughness

The Wire Electrical Discharge Machining (WEDM) process removes material from the workpiece surface through a sequence of electrical discharges that cause melting and evaporation [37]. Increasing the current in this process directly raises the energy per pulse, thereby

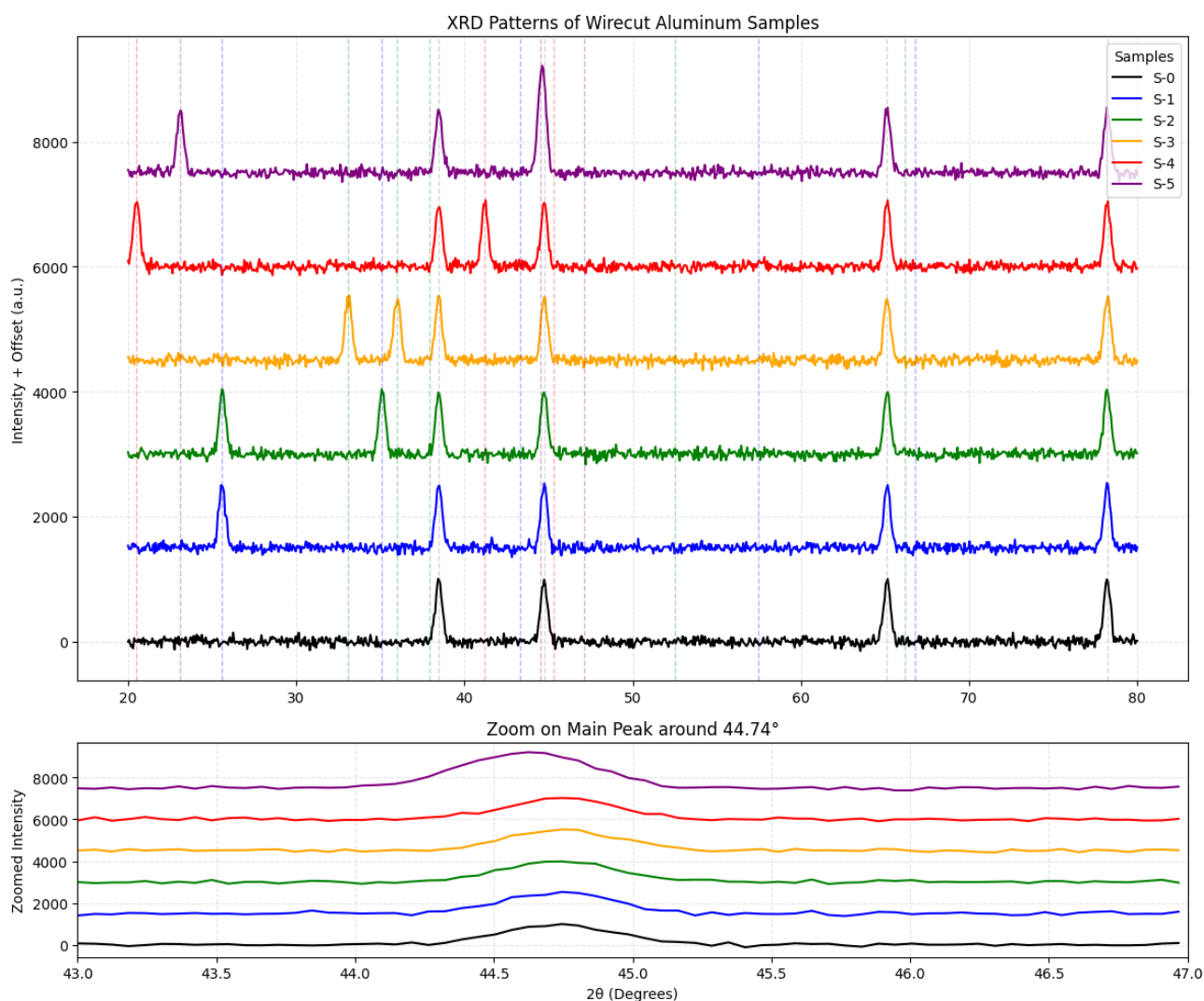


Fig. 3. XRD Analysis Results of the Tested Samples.



surface [38]. At low currents (S-0 and S-1), low-energy discharges produce a uniform surface with minimal damage; surface roughness ( $R_a$ ) remains in the range of approximately 1.8 to 3.5  $\mu\text{m}$ . These conditions result from controlled melting, limited evaporation, and rapid solidification without notable formation of adhered particles or microcracks, as shown in Fig. 4. At medium currents (S-2 and S-3), the increased pulse energy leads to more pronounced surface irregularities, with  $R_a$  values reaching about 3.2 to 3.5  $\mu\text{m}$ . This behavior corresponds to the presence of larger cavities and fine adhered particles on the surface [39, 40]. At higher currents (S-4 and S-5), although a further increase in roughness might be expected, experimental results reveal a relative decrease in  $R_a$  to approximately 3.1  $\mu\text{m}$  and, in some cases, as low as 2.5  $\mu\text{m}$ . This phenomenon can be attributed to surface remelting and partial smoothing of irregularities caused by excessive discharge energy. In fact, at very high currents, extensive localized melting can fill surface depressions with re-solidified material, which despite the potential for microcracking or porosity, produces a comparatively smoother surface [41]. Under these conditions, the interaction between molten material and the dielectric fluid, combined with rapid cooling, facilitates the removal of floating particles and minimizes their reattachment [42]. Therefore, the relationship between current intensity and surface roughness is not strictly linear, and at very high currents, due to remelting and dynamic surface smoothing phenomena, the surface roughness may decrease. These observations align with previous findings highlighting the role of dielectric fluid dynamics and cooling in determining the final surface morphology [41].

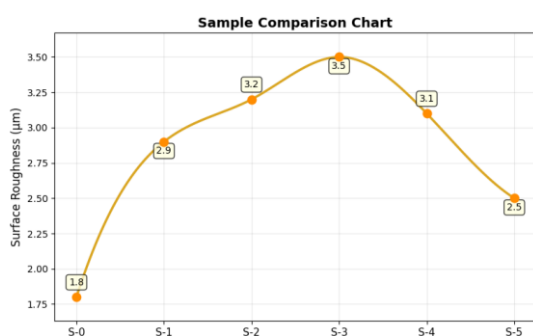


Fig. 4. Surface roughness measurement results after the WEDM process.

### 3.3. Surface hardness

The microhardness profiles obtained from the experimental data indicate a noticeable increase in hardness near the edges of the wire-cut specimens; however, the magnitude of this increase remains limited and controlled (approximately 6–8 HV compared to the reference sample). This pattern is consistent with the theoretical expectations for the heat-affected zone (HAZ) in aluminum, as shown in Fig. 5. Localized discharge energy at the edges induces surface microstructural changes and grain refinement, but due to the aluminum's high thermal conductivity and rapid heat dissipation, these effects do not penetrate deeply into the bulk material. In the central regions of the specimens (approximately 3 to 7 mm from the edges), a clear convergence of all profiles toward the hardness of the reference sample is observed. This convergence indicates that the thermal effects generated by the Wire-EDM process do not significantly penetrate into the bulk of the component, thereby preserving the core mechanical properties of the aluminum. From an engineering standpoint, this finding suggests that EDM-induced property changes are predominantly surface-limited. Consequently, in assessments of durability, fatigue, and mechanical behavior, the hardness should be considered as a surface-dependent parameter rather than a uniform property across the cross-section.

Previous studies on EDM and Wire-EDM have shown that increasing discharge energy (such as higher current intensity or longer pulse duration) is generally associated with higher surface hardness and a thicker modified layer. The underlying mechanisms include rapid quenching and grain refinement, surface oxidation, and, in some cases, element diffusion from the electrode wire. However, in aluminum, this phenomenon is typically moderate, excessive energy input may lead to adverse outcomes such as fine thermal cracks, porosity, or increased surface roughness, which could neutralize or even reverse the potential benefits of increased hardness in fatigue-sensitive.

### 3.4. Wear

Wear resistance is directly influenced by the combined

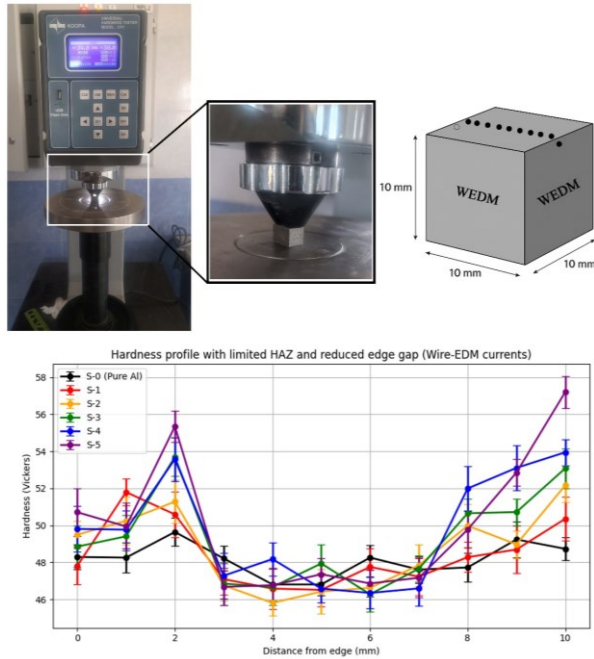


Fig. 5. Hardness measurement results after the WEDM process.

effects of surface hardness, roughness, and layer uniformity. At low current levels, a finer-grained, smooth, and hard surface layer forms, as shown in Fig. 6, exhibiting excellent resistance to abrasive contact, with mass loss typically remaining below 2.5 mg. At medium current levels, the concurrent decrease in hardness and increase in surface roughness raise the mass loss to approximately 4.5 mg. The formed oxide particles can act as secondary abrasives, further intensifying wear. At high current levels, the presence of a porous structure, semi-molten adherents, and thermal cracks results in surface brittleness and a significant acceleration of wear. The mass loss in these cases exceeds approximately 6.5 mg. Surfaces exhibiting such features typically have shorter lifespans in dynamic applications. Wear depth profiles, measured along a 4-mm path, reveal clear distinctions in the abrasive behavior of various aluminum samples machined under varying process conditions. The pure aluminum sample, which exhibited the greatest wear depth ( $\sim 70 \mu\text{m}$ ), demonstrated the lowest wear resistance — an expected outcome, as no microstructural modification, surface hardening, or thermal tempering occurs in this sample.

In contrast, samples processed by WEDM demonstrate varying wear behaviors depending on the

applied current. Medium currents result in partial surface refinement, the formation of a tempered layer, and moderate hardness, leading to a notable improvement in wear resistance. Conversely, at very high currents, increased pulse energy and the greater likelihood of localized burning degrade the surface structure, increasing brittleness and causing relatively higher

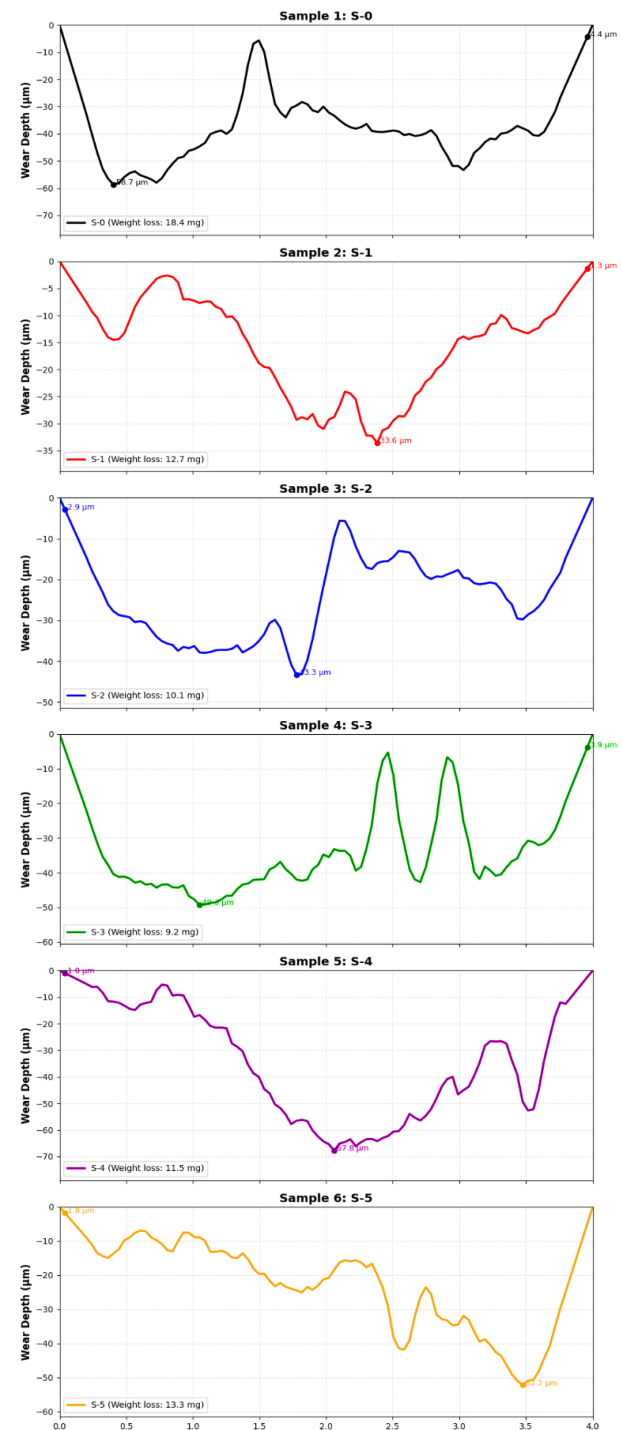


Fig. 6. Variations in wear depth along the sample path after the WEDM process.

wear. Point-wise analysis of the wear curves, including comparisons of maximum and minimum values, not only defines the wear fluctuation range but also facilitates evaluation of the uniformity of abrasive performance. The observation of minima and maxima indicates that wear in some samples, such as the third, is more stable and homogeneous, whereas samples like the fifth and the pure aluminum exhibit severe fluctuations in wear depth, likely due to surface structural discontinuities or localized hardness heterogeneity. These findings are particularly significant in industrial applications involving continuous contact and high friction (e.g., aerospace, automotive, and precision tooling components), as optimizing machining parameters can significantly enhance component lifespan and reduce maintenance and replacement costs.

### 3.5. Corrosion

This study investigated the effect of electrical discharge current intensity in the WEDM process on the corrosion resistance of aluminum alloy. The control sample (S-0), which was not machined, served as the baseline for comparison. According to the potentiodynamic polarization (PDP) curves, this sample exhibited the lowest corrosion current density ( $I_{\text{corr}} \approx 8 \times 10^{-7} \text{ A/cm}^2$ ) and the most negative corrosion potential ( $E_{\text{corr}} = -0.47 \text{ V}$ ), indicating high surface stability in the corrosive environment. With an increase in WEDM current up to 1 ampere (S-1), only a slight reduction in corrosion resistance was observed, suggesting that WEDM at this level does not significantly disrupt the natural aluminum oxide layer. However, at 2 A and 3 A (S-2, S-3), a marked decline in corrosion resistance occurred, as illustrated in Figs. 7 and 8, likely due to the formation of thermal cracks, increased surface roughness, and decreased homogeneity of the natural oxide layer on

aluminum.

Interestingly, sample S-4 displayed a nonlinear response: despite a higher current, it demonstrated better electrochemical behavior compared to S-2 and S-3. This improvement, evident from both PDP and electrochemical impedance spectroscopy (EIS) results, is likely associated with the reformation of protective layers due to more uniform heating and a more stable current discharge. The EIS curve showed that S-4 had a larger semicircle compared to the intermediate current samples, reflecting higher charge transfer resistance ( $R_{\text{ct}} \approx 1300 \text{ } \Omega$ ) and a lower double-layer capacitance. Conversely, sample S-5, machined at 5 A, experienced the most severe corrosion degradation, showing the smallest EIS semicircle and an  $I_{\text{corr}}$  value more than an order of magnitude higher than the others. This destructive behavior could result from melted zones, localized phase transformations, or the formation of brittle region. A magnified view of the interference region in the impedance plot indicated that although the differences between samples S-2 to S-5 appear subtle, they are in fact significant, necessitating detailed EIS analysis for accurate differentiation. These findings have direct implications for sensitive industries such as aerospace, petrochemical, and defense. In aerospace, aluminum components used in aircraft frames or satellite structures require precise machining without compromising corrosion resistance [43]. The results indicate that high-current WEDM, while capable of achieving good dimensional accuracy, can significantly reduce surface corrosion resistance and promote localized corrosion under humid or high-pressure conditions. Similarly, in the petrochemical industry, where acidic or chloride-rich environments prevail, even minor surface changes can drastically shorten component lifespan [44]. Therefore, defining an optimal

**Table 4.** Experimental results of the corrosion test

| Sample        | $\beta_a \text{ (V/dec)}$ | $\beta_c \text{ (V/dec)}$ | $i_{\text{corr}} \text{ (A/cm}^2\text{)}$ | $E_{\text{corr}} \text{ (V)}$ | $R_p \text{ (K}\Omega \cdot \text{cm}^2\text{)}$ | Corr. rate (mm/year) |
|---------------|---------------------------|---------------------------|---|-------------------------------|--|----------------------|
| S-0 (Pure Al) | 0.09                      | 0.11                      | $8\text{e-}07$                            | -0.47                         | 200  | 0.001                |
| S-1 (1A)      | 0.08                      | 0.1                       | $1\text{e-}06$                            | -0.45                         | 150  | 0.002                |
| S-2 (2A)      | 0.07                      | 0.09                      | $3\text{e-}05$                            | -0.44                         | 25   | 0.05                 |
| S-3 (3A)      | 0.065                     | 0.085                     | $1\text{e-}05$                            | -0.43                         | 50   | 0.015                |
| S-4 (4A)      | 0.055                     | 0.07                      | $5\text{e-}06$                            | -0.42                         | 80   | 0.008                |
| S-5 (5A)      | 0.05                      | 0.06                      | 0.0001                                    | -0.4                          | 10   | 0.2                  |



WEDM current window (under conditions comparable to S-4 or S-1) is essential to simultaneously ensure machining precision and corrosion stability, a crucial consideration in modern engineering design aimed at reducing maintenance costs and enhancing safety.

### 3.6. Microstructure of light microscope

The microscopic observations clearly reveal that discharge current in the wire-cut EDM process directly influences the melting behavior and localized thermal softening of aluminum. At lower currents (particularly in the first sample), the limited discharge energy produced shallow cavities and a narrow heat-affected zone. As the current increased to a moderate level (sample three), the higher discharge energy promoted deeper melting pits and a broader heat-affected zone. This behavior is consistent with the thermodynamic characteristics of aluminum, where medium current levels induce the highest thermal instability. At higher current levels

(samples four and five), however, evaporation and molten material ejection mechanisms appear to dominate, leading to a more dispersed energy distribution rather than concentrated melting. Consequently, the depth of the cavities decreased. Interestingly, in sample five, although the cavity depth was reduced, the lateral dimensions of the surface pits increased significantly. This can be attributed to excessive discharge energy, which facilitated widespread surface melting and lateral material flow. Such a change reflects a transition from localized melting to a broad, splash-like melting behavior. A comparison between the microscopic findings and surface roughness measurements demonstrates a strong correlation between surface morphology and roughness values. From the first to the third sample, surface roughness increased in parallel with the growth of cavity depth and the heat-affected zone. In contrast, in the fourth and fifth samples, despite the presence of large cavities in cross-sections, the surface roughness decreased, reaching its lowest level in sample five. This apparent contradiction can be explained by extensive remelting and partial filling of asperities. In other words, while higher discharge currents produced metallurgical changes and severe thermal effects, the resulting surface appeared smoother in terms of roughness. The metallography test supporting these observations are presented in Figs. 9 and 10.

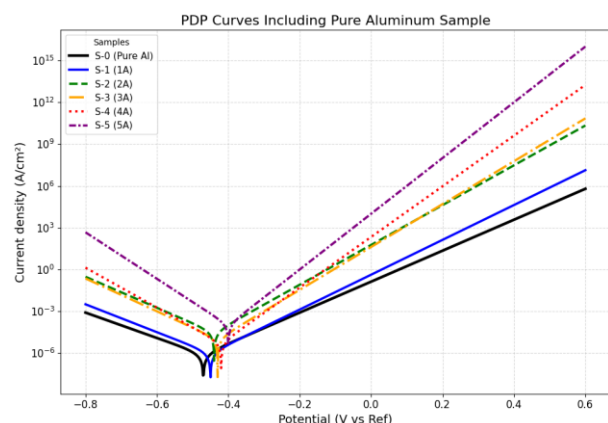


Fig. 7. Potentiodynamic polarization test results on machined surfaces.

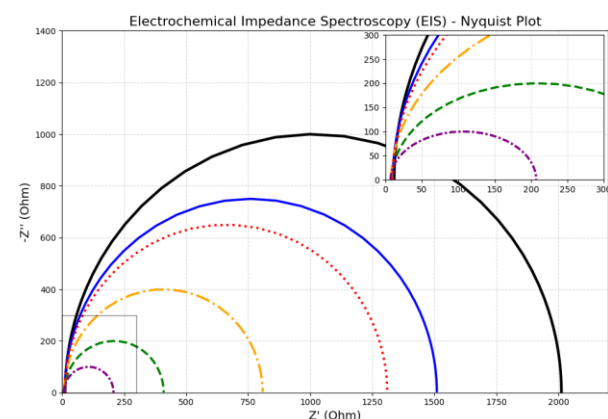


Fig. 8. Nyquist plot results on machined surfaces.

### 3.7. Energy consumption

According to the literature, current intensity is one of the main factors affecting energy consumption in WEDM. It is well established that the material removal rate (MRR) is directly proportional to pulse energy, which in turn depends on the current intensity. When machining is performed at lower current levels, less evaporation and melting occur between the electrodes, resulting in longer machining times and, consequently, higher operational costs [45]. As the current increases from 1 to 5 A, the specific energy consumption decreases due to the higher MMR and shorter cutting time. During the WEDM process, most of the input energy is transferred to the cathode, anode, and dielectric through thermal

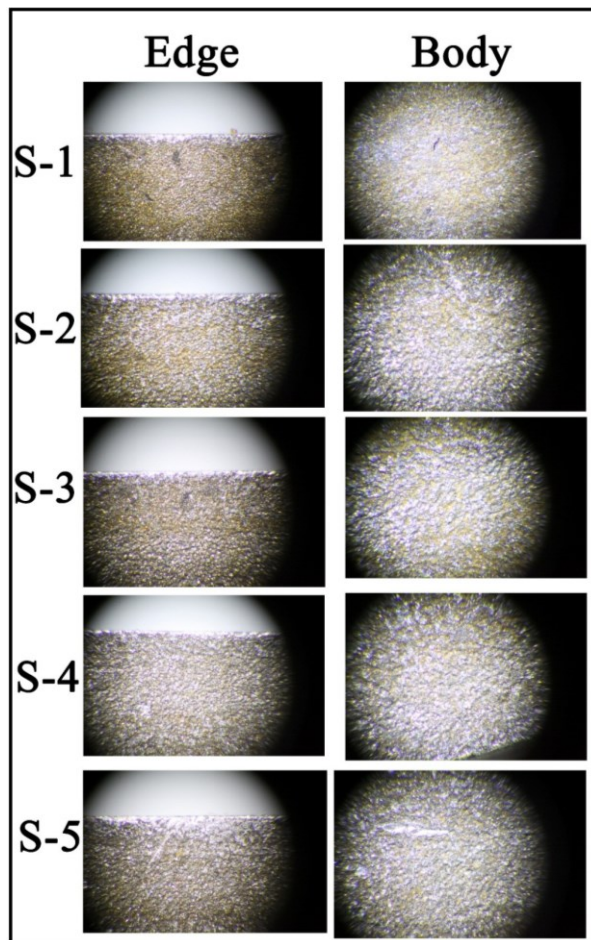


Fig. 9. Surface profilometry image illustrating the roughness distribution across the machined aluminum specimen.

conduction, while a small amount of energy is lost via thermal radiation and convection. The distribution of energy among the tool electrode, dielectric fluids and workpiece depends on several parameters including thermal diffusivity, density, melting temperature, heat capacity and thermal conductivity of both materials. Therefore, the total energy of the process can be expressed by Eq. (2) [46]:

$$E_{total} = E_w + E_e + E_d + E_r \quad (2)$$

Where  $E_w$  and  $E_e$  represent the energy distributed in the workpiece and the tool electrode, respectively,  $E_d$  is the energy absorbed by the dielectric fluids; and  $E_r$  is the energy consumed by radiation, light and sound. The energy transferred into the workpiece ( $E_w$ ) is then used to remove the material and is carried away with the waste, contributing positively to process efficiency. In

contrast, the energy absorbed by the tool electrode ( $E_e$ ) causes electrode wear, leading to energy loss and reducing the high precision of the WEDM process. Therefore, to enhance effective energy efficiency under identical pulse condition, minimizing unnecessary energy dissipation is a useful approach to improving WEDM performance and reducing overall energy consumption. The material removal rate (productivity) per unit of input energy has a significant impact on the energy consumption of the process, implying that in WEDM, the primary goal is to increase MRR and reduce machining time while lowering total energy consumption. According to previous research, the influence of pulse energy variations on specific energy consumption (SEC) can be expressed by Eq. (3) [46]:

$$SEC = E/V \quad (3)$$

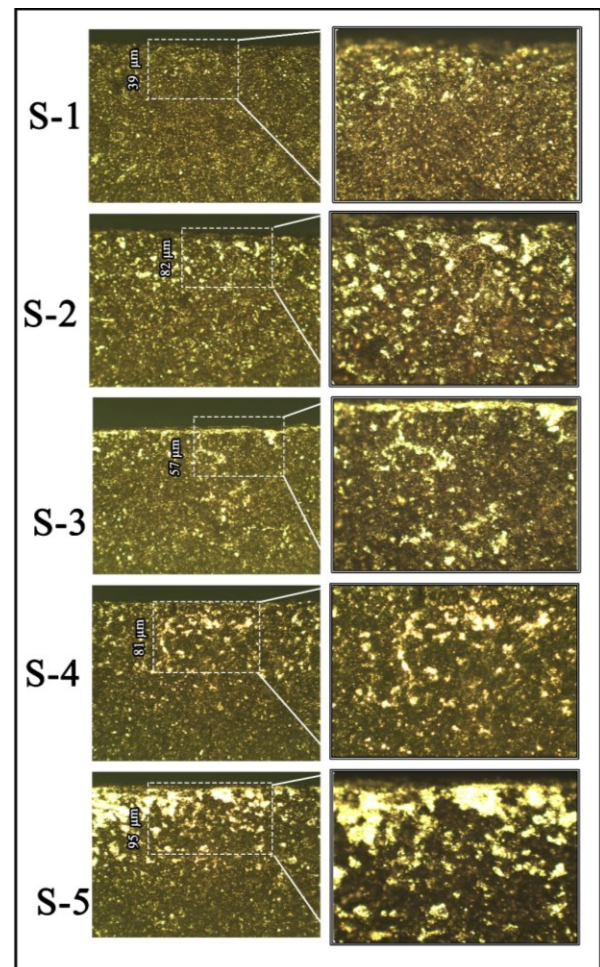


Fig. 10. Optical micrograph of the wire-cut EDM surface showing the heat-affected zone (HAZ) with highlighted measurements of cavity depth and lateral dimensions.

Table 5. Consolidated research results

| Sample        | Current intensity (A) | Surface roughness (Ra, $\mu\text{m}$ ) | Hardness (Brinell) | Wear rate (mg) | Corrosion rate (mm/year) |
|---------------|-----------------------|--|--------------------|----------------|--------------------------|
| S-0 (Pure Al) | -                     | $0.2 \pm 0.02$                         | $45 \pm 2$         | 18.4           | 0.001                    |
| S-1 (1A)      | 1                     | $1.8 \pm 0.1$                          | $52 \pm 3$         | 12.7           | 0.002                    |
| S-2 (2A)      | 2                     | $2.5 \pm 0.15$                         | $58 \pm 2$         | 10.1           | 0.05                     |
| S-3 (3A)      | 3                     | $3.2 \pm 0.2$                          | $75 \pm 5$         | 9.2            | 0.015                    |
| S-4 (4A)      | 4                     | $4.0 \pm 0.25$                         | $70 \pm 3$         | 11.5           | 0.008                    |
| S-5 (5A)      | 5                     | $5.5 \pm 0.3$                          | $65 \pm 4$         | 13.3           | 0.2                      |

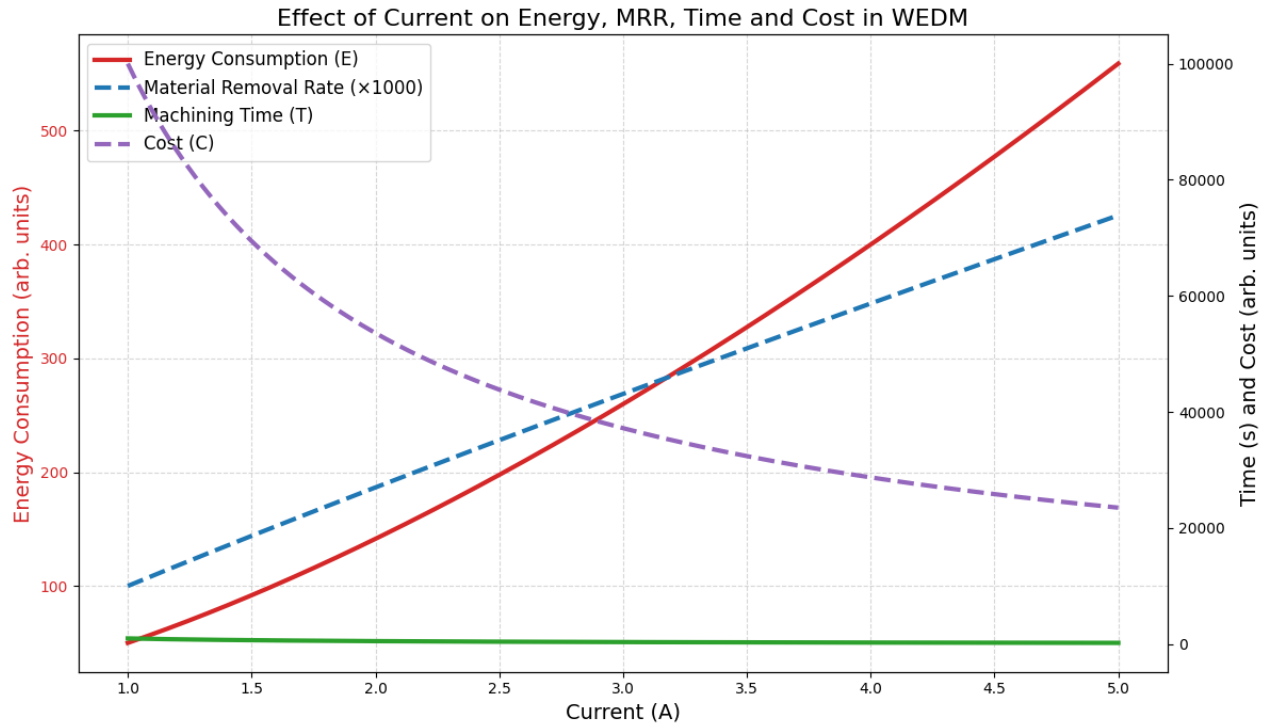


Fig. 11. Consolidated graphical results.

The combination of pulse width and peak current determines the spark energy, which can be expressed by Eq. (4) [46]:

$$E = I \times U \times T_{on} \quad (4)$$

Where  $I$  is the current,  $U$  is the spark gap setting voltage, and  $T_{on}$  is the pulse on time. In addition, the  $MRR$  is defined as the volume of material removed per unit time during the EDM process. Therefore, the removed material volume  $V$  can be calculated using Eq. (5) [46]:

$$V = MRR = V_c \times T_h \quad (5)$$

Where  $V_c$  is the average feed rate (m/s), and  $T_h$  is the thickness of the workpiece. Therefore, increasing the metal removal rate is an effective method to reduce SEC

and reduce energy consumption, as it improves the proportion of energy effectively absorbed by the workpiece.

It seems that a current between approximately 2.5 and 3 A provides the best energy efficiency and surface quality for aluminum, while higher currents not only reduce surface quality but also increase energy consumption and operating costs [13]. As shown in Fig. 11, selecting a lower current saves energy but extends longer machining times and increased time-related costs; conversely, higher currents shorten machining time but greatly increase energy costs. All summarized results are presented in Table 5. Therefore, in industrial applications, it is recommended to choose a current intensity within this optimal range to maintain quality and speed while minimizing costs and energy consumption, thereby achieving economic optimization.

#### 4. Conclusions

The results of this study demonstrated that the electrical discharge current in the wire electrical discharge machining (WEDM) process plays a decisive role in determining surface quality, tribological behavior, and energy efficiency of aluminum. Increasing the current from 1 to 5 amperes led to a continuous rise in surface roughness, a decrease in hardness, an increase in wear and corrosion rates, and ultimately higher specific energy consumption. These changes were caused by the increased discharge energy per pulse and more intense thermal effects on the workpiece surface, resulting in the formation of resolidified layers, porous structures, and, in some cases, unstable surface morphologies.

A comprehensive analysis of these effects suggests that low to medium current levels (approximately 2 to 3 amperes) provide the optimal balance among surface quality, mechanical resistance, and energy efficiency. These findings can serve as practical guidance for optimizing WEDM parameters in the machining of aluminum components for precision and surface-quality-sensitive industries.

1. Surface roughness progressively increased with higher discharge current (1- 5A); Ra rose from about 1.2 to 4.9  $\mu\text{m}$  due to the enlargement and intensification of melting cavities and the formation of heterogeneous surface layers.
2. Surface hardness decreased 72 to 56 HV as current increased, mainly due to slower cooling rates, thicker molten layers, and the development of coarse-grained, brittle microstructures.
3. Wear resistance was higher at lower currents; as the current increased, the surface became softer and rougher, leading to a significant rise in mass loss during wear tests (from 2.2 to 6.8 mg).
4. The corrosion rate increased with higher current intensity. At elevated currents, the formation of porous and unstable surface layers led to corrosion rates rising up to 0.15 mm/year, indicating a significant decline in corrosion resistance.
5. Specific energy consumption initially decreased up to 3 amperes (the optimal point) but increased again at higher currents, due to reduced efficiency of

electrical discharges and a higher frequency of unsuccessful or nonproductive discharges.

6. The optimal current range for aluminum WEDM is recommended between 2.5 and 3 amperes, providing a balance between surface quality, mechanical durability, corrosion resistance, and energy efficiency.

#### Acknowledgement

The authors sincerely thank Ms. Zahra Golkhar (Iran-Gonabad) and Ms. Maryam Nouri (Iran-Gonabad) for their invaluable support and contributions to this research. Their assistance and encouragement were instrumental in the successful completion of this work.

#### Authors' contributions

**R. A. Mahdavinjad:** Conceptualization, Methodology, Software, Validation, Writing - Review & Editing

**S. M. Sedehi:** Software, Investigation, Formal analysis, Original Draft, Data Curation

**S. N. Sharifi:** Software, Resources, Writing - Review & Editing, Supervision

**A. Dastmard:** Project administration, Writing - Review & Editing

#### Conflict of interest

The authors declare that they have no financial interests or personal relationships that could have influenced the results of this study.

#### Funding

This research was conducted without any financial support.

#### 5. References

- [1] Chandel, R., Sharma, N., & Bansal, S. A. (2021). A review on recent developments of aluminum-based hybrid composites for automotive applications. *Emergent Materials*, 4(5), 1243–1257. <https://doi.org/10.1007/s42247-021-00186-6>
- [2] Lakshmanan, K., Pandian, P., Sivaprakasam, R., & Sundaram, K. (2025). Studies on progress of aluminum-based composites for automotive applications and its damping characteristics – A review. *Mechanics of*



- Advanced Composite Structures*, 12(1), 25–42.  
<https://doi.org/10.22075/mac.2024.32547.1589>
- [3] Sharma, S. K., Gajević, S., Sharma, L. K., Pradhan, R., Sharma, Y., Miletić, I., & Stojanović, B. (2024). Progress in aluminum-based composites prepared by stir casting: Mechanical and tribological properties for automotive, aerospace, and military applications. *Lubricants*, 12(12), 421. <https://doi.org/10.3390/lubricants12120421>
- [4] Hickman, A. L., Chaudhuri, R., Bader, S. J., Nomoto, K., Li, L., Hwang, J. C., Xing, H. G., & Jena, D. (2021). Next generation electronics on the ultrawide-bandgap aluminum nitride platform. *Semiconductor Science and Technology*, 36(4), 044001.  
<https://doi.org/10.1088/1361-6641/abe5fd>
- [5] Dutta, K., Duarah, R., Purbey, R., Jayaramudu, J., & Das, M. R. (2025). Development of biodegradable high-alumina clay-modified poly (butylene adipate-co-terephthalate) composites for sustainable packaging applications. *Journal of Applied Polymer Science*, e56680. <https://doi.org/10.1002/app.56680>
- [6] Xuepeng, W. A., Zhen, L. I., Xueli, Q. I., & Haonan, X. U. (2024). Preparation methods and research progress of continuous alumina fibers. *Journal of Ceramics*, 45(6), 1125–1135.  
<https://doi.org/10.13957/j.cnki.tcxb.2024.06.005>
- [7] Arunraja, K. M., Muthugounder, P., Karthikeyan, S., Ganesan, S., Gowrishankar, A., & Muruganandhan, B. P. (2025, June). Influences of jute fiber and alumina nanoparticles on behaviour of polyester composite synthesized via hand layup route. In *AIP Conference Proceedings* (Vol. 3267, No. 1, p. 020290). AIP Publishing LLC. <https://doi.org/10.1063/5.0264673>
- [8] Rogachev, S. O., Naumova, E. A., Karelin, R. D., Andreev, V. A., Perkas, M. M., Yusupov, V. S., & Khatkevich, V. M. (2021). Structure and mechanical properties of Al–Ca–Mn–Fe–Zr–Sc eutectic aluminum alloy after warm equal channel angular pressing. *Russian Journal of Non-Ferrous Metals*, 62, 293–301.  
<https://doi.org/10.3103/s1067821221030123>
- [9] Samuel, A. U., Araoyinbo, A. O., Elewa, R. R., & Biodun, M. B. (2021). Effect of machining of aluminium alloys with emphasis on aluminium 6061 alloy – A review. In *IOP Conference Series: Materials Science and Engineering* (Vol. 1107, No. 1, p. 012157). IOP Publishing.  
<https://doi.org/10.1088/1757-899x/1107/1/012157>
- [10] Santos, D. B. P., Maia, L. H. A., Martins, P. S., Ba, E. C. T., Vieira, V. F., Shigaki, Y., Fernandes, G. H. N., & Santos, S. C. (2025). Dynamic and dimensional evaluation of robot applications in the drilling process in Al–Mg–Si 6351 T6 aluminum alloy. *The International Journal of Advanced Manufacturing Technology*, 1–25.  
<https://doi.org/10.1007/s00170-025-15054-4>
- [11] Sable, Y. S., Dharmadhikari, H. M., More, S. A., & Sarris, I. E. (2025). Exploring artificial neural network techniques for modeling surface roughness in wire electrical discharge machining of aluminum/silicon carbide composites. *Journal of Composites Science*, 9(6), 259. <https://doi.org/10.3390/jcs9060259>
- [12] Kulandaiyappan, N. K., Stanislaus Arputharaj, B., Rajendran, P., Raja, V., & Karuppasamy, A. (2025). Development of statistical and soft computing regression models for WEDM machining of aluminum composites. *International Journal on Interactive Design and Manufacturing (IJIDeM)*, 19(5), 3707–3723.  
<https://doi.org/10.1007/s12008-024-02017-4>
- [13] Mahdich, M. S., Nazari, F., Ahmed Mussa, T., & Torfy Salehi, H. (2023). A study on stamping of airliner's tail connector part through FEM simulation. *Journal of Simulation and Analysis of Novel Technologies in Mechanical Engineering*, 15(3), 5–13.  
<https://doi.org/10.71939/jsme.2023.1092088>
- [14] Mahdich, M. S. (2023). Improving surface integrity of electrical discharge machined ultra-fine grain Al-2017 by applying RC-type generator. *Proceedings of the Institution of Mechanical Engineers, Part E: Journal of Process Mechanical Engineering*.  
<https://doi.org/10.1177/09544089231202329>
- [15] Uday Kiran Kandala, A. V., Solomon, D. G., & Arulraj, J. J. (2022). Advantages of Taguchi method compared to response surface methodology for achieving the best surface finish in wire electrical discharge machining (WEDM). *Journal of Mechanical Engineering (JMEchE)*, 19(1), 185–200.  
<https://doi.org/10.24191/jmeche.v19i1.19696>
- [16] Ali, M. A., Mufti, N. A., Sana, M., Tlija, M., & Khan, A. M. (2025). An intrinsic investigation on high-speed wire-EDM for surface integrity, kerf width, and cutting performance of hybrid composite. *Materials Today Communications*, 42, 111548.  
<https://doi.org/10.1016/j.mtcomm.2025.111548>
- [17] Mussada, E. K., Hua, C. C., & Rao, A. P. (2025). Surface and subsurface hardenability of AA6061-T6 aerospace alloy machined by WEDM. *Aircraft Engineering and Aerospace Technology*, 97(5), 542–548.  
<https://doi.org/10.1108/aeat-04-2024-0091>
- [18] Dhoria, S. H., Subbaiah, K. V., Rao, V., Thulasiram, R., Bhowmik, A., & Santhosh, A. J. (2025). Experimental investigation of wire EDM on squeeze cast Al6351/Gr/SiC hybrid metal matrix composites: A Taguchi–GRA-based optimization framework. *AIP Advances*, 15(4). <https://doi.org/10.1063/5.0267581>
- [19] Chen, S. T., & Huang, L. W. (2022). A micro-energy W-EDM power source based on high-frequency spark erosion for making diamond heat-sink arrays. *International Journal of Precision Engineering and*



- Manufacturing-Green Technology*, 9(5), 1267–1283.  
<https://doi.org/10.1007/s40684-021-00396-7>
- [20] Solomon, J. M., Selvakumar, G., Kumar, S. S., & Narayanasamy, P. (2024). Experimental investigation of wire electrical discharge machining parameters on WE43 magnesium alloy. *Metallurgical Research & Technology*, 121(2), 203.  
<https://doi.org/10.1051/metal/2024005>
- [21] Siyoum, Y. B., Kindie, F. G., Gebeyehu, M. A., Chanie, S. E., Yeshiwas, T. A., & Zelalem, Y. A. (2025). Comparative optimization of wire-cut EDM parameter for enhancing surface finish and machining time on stainless steel: A machine learning, genetic algorithms, teaching–learning-based optimization, and multi-objective Jaya approach. *The International Journal of Advanced Manufacturing Technology*, 137(9), 5339–5362. <https://doi.org/10.1007/s00170-025-15450-w>
- [22] Sen, B., Dasgupta, A., & Bhowmik, A. (2024). Optimizing wire-cut EDM parameters through evolutionary algorithm: A study for improving cost efficiency in turbo-machinery manufacturing. *International Journal on Interactive Design and Manufacturing (IJIDeM)*.  
<https://doi.org/10.1007/s12008-024-02001-y>
- [23] Zheng, J., Qi, T., Hu, X., Pan, Q., Zhang, Z., Guan, A., Ling, W., Peng, T., Wu, J., & Wang, W. (2024). Energy consumption assessment and economic analysis of a novel sustainable electro-machining auxiliary system. *Applied Energy*, 357, 122521.  
<https://doi.org/10.1016/j.apenergy.2023.122521>
- [24] Kokare, S., Oliveira, J. P., Santos, T. G., & Godina, R. (2023). Environmental and economic assessment of a steel wall fabricated by wire-based directed energy deposition. *Additive Manufacturing*, 61, 103316.  
<https://doi.org/10.1016/j.addma.2022.103316>
- [25] Takele, Y. F., & Woldeyohannes, A. D. (2025). Optimal material selection for high temperature tribological application: An integrated multi-criteria decision study. *Discover Materials*, 5(1), 33.  
<https://doi.org/10.1007/s43939-025-00209-7>
- [26] Zhang, P., Yue, X., Wang, S., Sun, Y., Zhou, H., & Zhang, J. (2024). Characterization of surface integrity of 7075-T6 aluminum alloy subjected to microbiologically induced corrosion during high-speed machining. *Journal of Alloys and Compounds*, 1008, 176843.  
<https://doi.org/10.1016/j.jallcom.2024.176843>
- [27] Muhammad, A. K., Mohammed, T. W., & Resan, K. K. (2024). Chemical machining of aluminum alloy 2024: The critical roles of temperature and solution concentration in enhancing corrosion rate and surface texture. *Journal of Engineering and Technological Sciences*, 56(4), 489–498.  
<https://doi.org/10.5614/j.eng.technol.sci.2024.56.4.5>
- [28] Alam, M. A., Jahan, A., Suzuki, E., & Yashiro, H. (2024). Surface morphology and corrosion behavior of pure aluminum and its alloys in aqueous sulfuric acid medium. *Engineering Reports*, 6(4), e12750.  
<https://doi.org/10.1002/eng2.12750>
- [29] Kiyak, M. (2022). Investigation of effects of cutting parameters on surface quality and hardness in the wire-EDM process. *The International Journal of Advanced Manufacturing Technology*, 119(1), 647–655.  
<https://doi.org/10.1007/s00170-021-08302-w>
- [30] Reddy, M. C., Rao, K. V., & Suresh, G. (2021). An experimental investigation and optimization of energy consumption and surface defects in wire cut electric discharge machining. *Journal of Alloys and Compounds*, 861, 158582.  
<https://doi.org/10.1016/j.jallcom.2020.158582>
- [31] de Argandoña, E. S., Zabala, A., Galdos, L., & Mendiguren, J. (2020). The effect of material surface roughness in aluminum forming. *Procedia Manufacturing*, 47, 591–595.  
<https://doi.org/10.1016/j.promfg.2020.04.182>
- [32] DIN EN ISO 6506-1:2015-02. (2015). *Metallic materials – Brinell hardness test – Part 1: Test method*. Beuth Verlag GmbH, Berlin, Germany.
- [33] Sedehi, S. M., Samarghandi, M., Samarghandi, A., & Maraki, M. (2024). The effect of simple shear extrusion on the microstructure and surface properties of aluminum components produced by powder metallurgy. *Iranian Journal of Materials Forming*, 11(1), 24–33.  
<https://doi.org/10.22099/ijmf.2024.49501.1282>
- [34] Haynes, G. (1990). Review of laboratory corrosion tests and standards. In *Corrosion Testing and Evaluation: Silver Anniversary Volume*. ASTM International.  
<https://doi.org/10.1520/stp39195s>
- [35] Mohammed, A. A., Khodair, Z. T., & Khadom, A. A. (2020). Preparation and investigation of the structural properties of  $\alpha$ -Al<sub>2</sub>O<sub>3</sub> nanoparticles using the sol-gel method. *Chemical Data Collections*, 29, 100531.  
<https://doi.org/10.1016/j.cdc.2020.100531>
- [36] Wang, X., Qiang, D., Hosier, I., Zhu, Y., Chen, G., & Andritsch, T. (2020). Effect of water on the breakdown and dielectric response of polypropylene/nano-aluminium nitride composites. *Journal of Materials Science*, 55(21), 8900–8916.  
<https://doi.org/10.1007/s10853-020-04635-1>
- [37] Ho, K., Newman, S., Rahimifard, S., & Allen, R. (2004). State of the art in wire electrical discharge machining (WEDM). *International Journal of Machine Tools and Manufacture*, 44, 1247–1259.  
<https://doi.org/10.1016/j.ijmachtools.2004.04.017>
- [38] Roy, A., Narendranath, S., & Pramanik, A. (2020). Effect of peak current and peak voltage on machined surface morphology during WEDM of TiNiCu shape memory

- alloys. *Journal of Mechanical Science and Technology*, 34, 3957–3961.  
<https://doi.org/10.1007/s12206-020-2205-x>
- [39] Ghanem, F., Braham, C., & Sidhom, H. (2003). Influence of steel type on electrical discharge machined surface integrity. *Journal of Materials Processing Technology*, 142, 163–173.  
[https://doi.org/10.1016/S0924-0136\(03\)00572-7](https://doi.org/10.1016/S0924-0136(03)00572-7)
- [40] Jangra, K. K. (2014). An experimental study for multi-pass cutting operation in wire electrical discharge machining of WC-5.3% Co composite. *International Journal of Advanced Manufacturing Technology*, 76, 971–982. <https://doi.org/10.1007/s00170-014-6218-4>
- [41] Chaudhari, R., Vora, J. J., Patel, V., Lacalle, L. L., & Parikh, D. M. (2020). Effect of WEDM process parameters on surface morphology of nitinol shape memory alloy. *Materials*, 13(21), 4943.  
<https://doi.org/10.3390/ma13214943>
- [42] Magabe, R., Sharma, N., Gupta, K., & Davim, J. P. (2019). Modeling and optimization of Wire-EDM parameters for machining of Ni55.8Ti shape memory alloy using hybrid approach of Taguchi and NSGA-II. *International Journal of Advanced Manufacturing Technology*, 102, 1703–1717.  
<https://doi.org/10.1007/s00170-019-03287-z>
- [43] Zhang, P., Yue, X., Gao, Y., Wang, S., Sun, Y., Zhou, H., & Zhang, J. (2024). Research on the surface corrosion behavior of 7075-T6 aluminum alloy during high-speed machining and particle inclusion water jet composite reinforcement. *Vacuum*, 219, 112700.  
<https://doi.org/10.1016/j.vacuum.2023.112700>
- [44] Sun, X., & Hu, J. (2023). Corrosion types and measures for petrochemical equipment. *International Journal of Energy*, 3(2). <https://doi.org/10.54097/ije.v3i2.002>
- [45] Kuo, C. G., Hsu, C. Y., Chen, J. H., & Lee, P. W. (2017). Discharge current effect on machining characteristics and mechanical properties of aluminum alloy 6061 workpiece produced by electric discharging machining process. *Advances in Mechanical Engineering*, 9(11), 1687814017730756.  
<https://doi.org/10.1177/1687814017730756>
- [46] Zhang, Z., Yu, H., Zhang, Y., Yang, K., Li, W., Chen, Z., & Zhang, G. (2018). Analysis and optimization of process energy consumption and environmental impact in electrical discharge machining of titanium superalloys. *Journal of Cleaner Production*, 198, 833–846.  
<https://doi.org/10.1016/j.jclepro.2018.07.053>